

# The topology of the triple Pomeron vertex in $\mathcal{N} = 4$ SYM

J. Bartels, M. Hentschinski, A.-M. Mischler

*II. Institute for Theoretical Physics, Hamburg University, Germany*

November 9, 2018

## Abstract

We investigate, within  $\mathcal{N} = 4$  SYM, the high energy behavior in the triple Regge limit of a six point correlator of  $R$ -currents. Using the leading logarithmic approximation, we sum all diagrams whose color lines fit onto the surface of a sphere. We find three distinct classes of graphs, and one of them contains the triple Pomeron vertex known from QCD. We present results which, within the AdS/CFT correspondence, can be compared with scattering amplitudes in the dual string theory.

## 1 Introduction

Within the AdS/CFT correspondence [1], which relates  $\mathcal{N} = 4$  Supersymmetric Yang Mills quantum field theory (SYM) in four dimensions to a string theory in an  $AdS_5 \otimes S_5$  space, correlators of  $R$ -currents provide a useful tool for investigating the Regge limit, in particular the correspondence between the BFKL Pomeron in  $\mathcal{N} = 4$  SYM and the graviton on the string side.

In the simplest case, the elastic scattering of two  $R$ -currents, both ends of the correspondence have been investigated in leading order. On the gauge theory side, the supersymmetric impact factors consisting of the sum of a fermion and of a scalar loop in the adjoint representation of the gauge group have been computed [2], and it has been verified that the high energy behavior is described by the BFKL Pomeron [3]. On the string side, the leading contribution in the zero slope limit is given by the Witten diagram with graviton exchange [4]. Beyond the zero slope limit, the graviton is believed to reggeize [5].

A next step along this line is the six point function of  $R$ -currents in the triple Regge limit. In this kinematic limit one expects to see the triple Pomeron vertex which represents, besides the BFKL kernel, another fundamental element of high energy QCD: it describes the splitting of a BFKL Pomeron into two BFKL Pomerons. On the string side, one expects the graviton self interaction to play the analogous role. For QCD - with fermions in the fundamental representation and with the electromagnetic current in place of the  $R$ -current - the six point function at finite  $N_c$  has first been studied in [6]. As the main result, the triple Pomeron vertex has been identified, which by now has been derived in several other approaches. In [7] the case of the six point function of  $R$ -currents in  $\mathcal{N} = 4$  SYM has been studied for finite  $N_c$ : whereas the triple Pomeron vertex remains the same as in the non-supersymmetric case, a new contribution to the six point correlator appears which results from the adjoint color representation of the particles and has no counterpart in QCD.

Another line of interest is the integrability [8] of the BKP equation [9]: since in the leading logarithmic approximation there is no difference between QCD and its supersymmetric generalization,  $\mathcal{N} = 4$  SYM, one expects that the integrability which has been discovered for the large- $N_c$  limit of QCD in fact is 'inherited' from  $\mathcal{N} = 4$  SYM. The environment where the large- $N_c$  limit of BKP states can be studied are higher order current correlators, e.g. the eight point function in a suitable multi-Regge limit. Within the AdS/CFT correspondence, the counterpart of the BKP states and the role of integrability on the string side has not been addressed at all.

Recently, an attempt has been made to formulate these high energy calculations within a topological approach: in the large- $N_c$  limit, the color structure of scattering amplitudes can be attributed to surfaces: spheres, planes, cylinders, pair-of-pants, etc. The simplest examples include, in QCD with fermions in the fundamental representation, multi-gluon scattering amplitudes in the plane and the BFKL Pomeron on the cylinder. In [10] also the six point correlator of electromagnetic currents has been studied in the large- $N_c$  limit by summing diagrams whose color structure lies on the surface of a pair-of-pants. The study of these color diagrams provides a new view on the reggeization of the gluon and on the triple Pomeron vertex: whereas the reggeization can be understood as a feature of planar QCD, the triple Pomeron vertex requires a non-planar structure, reminiscent of the non-planar Mandelstam cross diagram.

When turning, from QCD with fundamental fermions, to  $\mathcal{N} = 4$  SYM with fermions and scalars in the adjoint representation, one encounters changes in the topology of the surfaces and in the structure of color graphs. The first example is the BFKL Pomeron which lies on the surface of a sphere with zero boundaries. Apart from this the form of the impact factor stays the same. In the present paper we address in the large- $N_c$  limit a six point correlator of  $R$ -currents in  $\mathcal{N} = 4$  SYM in the topological approach. We sum graphs whose color structure belongs to a specific deformation of a sphere, corresponding to the pair-of-pants investigated in [10].

We first review the color structure of Feynman diagrams in the large- $N_c$  limit and define the classes of graphs which we are going to sum. Our final result for the large- $N_c$  limit consists of three terms which represent three distinct classes of color diagrams on the surface of the deformed sphere.

## 2 Topology of graphs in $\mathcal{N} = 4$ SYM

It may be useful to recapitulate the large- $N_c$  limit of QCD with fermions in the fundamental representation, and to recall a few features of the classical paper of 't Hooft [11]. Starting from the Fierz identity

$$(g^a)_j^i (g^a)_l^k = \delta_l^i \delta_j^k - \frac{1}{N_c} \delta_j^i \delta_l^k, \quad (1)$$

where  $(g^a)_j^i$  denote the  $SU(N_c)$  generators in the fundamental representation (with the normalization  $\text{tr}(g^a g^b) = \delta^{ab}$ ), and from the identity

$$f^{abc} = \frac{1}{i\sqrt{2}} [\text{tr}(g^a g^b g^c) - \text{tr}(g^c g^b g^a)], \quad (2)$$

one is lead to draw, in the large- $N_c$  limit, color diagrams with the following elements:

(i) for each quark in the fundamental representation, a single line with an arrow, indicating the flow from the upper to the lower index,

$$\delta_j^i = i \longrightarrow j; \quad (3)$$

(ii) for each inner gluon a double line

$$\delta_l^i \delta_j^k = \begin{array}{c} i \longrightarrow l \\ j \longleftarrow k \end{array}; \quad (4)$$

(iii) for each triple gluon vertex

$$f^{abc} = \frac{1}{i\sqrt{2}} [\text{tr}(g^a g^b g^c) - \text{tr}(g^c g^b g^a)]. \quad (5)$$

As a result, each graph turns into a network of double and single lines. The resulting diagrams represent only the color factors. A usual Feynman diagram represents both the color factors and the momentum part. In the double line notation the momentum part has to be written separately.

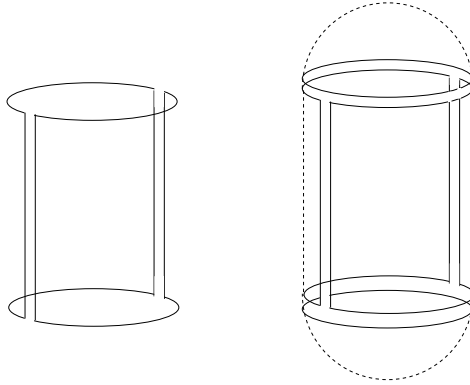


Figure 1: Cylinder topology for the  $2 \rightarrow 2$  scattering in QCD (left) and in  $\mathcal{N} = 4$  SYM (right)

The double line diagrams can be drawn on a two-dimensional surface with Euler number  $\chi = 2 - 2h - b$ , where  $h$  is the number of handles of the surface, and  $b$  the number of boundaries or holes. A closed color-loop always delivers a factor  $N_c$ , and with the quark in the fundamental representation of  $SU(N_c)$ , a closed quark-loop is  $1/N_c$  suppressed, compared to a corresponding gluon-loop, and leads to a boundary. For an arbitrary vacuum graph  $T$  one arrives at the following expansion in  $N_c$

$$T = \sum_{h,b}^{\infty} N_c^{2-2h-b} T_{h,b}(\lambda) \quad (6)$$

where

$$\lambda = g^2 N_c \quad (7)$$

is the 't Hooft-coupling which is held fixed, while  $N_c$  is taken to infinity.

In the expansion Eq.(6) which matches the loop expansion of a closed string theory with the string coupling  $1/N_c$ , the leading- $N_c$  diagrams are those that have the topology of a sphere: zero handles and zero boundaries,  $h = b = 0$ . If quarks are included, the leading diagrams have the topology of a disk, i.e. the surface with zero handle and one boundary,  $h = 0, b = 1$ , fits on the plane, with the boundary as the outermost edge. Diagrams with two boundaries and zero handles can be drawn on the surface of a cylinder, those with three boundaries on the surface of a pair-of-pants. Boundaries are also obtained by removing, from the sphere, one or more points. Removing one point, one obtains the disk, which can be drawn on the plane, and by identifying the removed point with infinity, the graphs can be drawn on the (infinite) plane. Removing two points we obtain the cylinder and so on. By definition, the expansion Eq.(6) is defined for vacuum graphs. However, from the earliest days on [12], the large- $N_c$  limit has been also applied to the scattering of colored objects. In order to consider the topological expansion of an amplitude with colored external legs, one needs to embed it into a vacuum graph which then defines the topological expansion of an amplitude with colored external legs.

In the large- $N_c$  limit of high energy QCD, quark scattering amplitudes are drawn on a plane; in particular, one can show that the BFKL bootstrap condition is satisfied on the plane (zero handles, one boundary). Next, for the BFKL Pomeron the color diagrams lie on the surface of a cylinder (zero handles, two boundaries), (Fig.1, left), and the triple Pomeron vertex is obtained from diagrams which fit on the pair-of-pants surface (zero handles, three boundaries), (Fig.2 and Fig.3, left).

Let us now turn to  $\mathcal{N} = 4$  SYM where fermions and scalars belong to the adjoint representation and therefore are represented by double lines, in the same way as the gauge bosons. Now fermion loops no longer define boundaries and therefore cannot be used to define separate topologies. As an example, in QCD with fundamental quarks the diagrams of the BFKL Pomeron fit onto the surface of

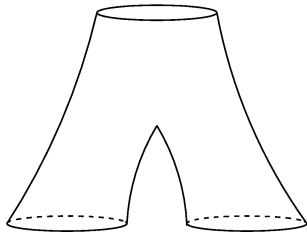


Figure 2: Pair-of-pants topology

a cylinder (Fig.1, left): the closed quark loops at the top and at the bottom define the two boundaries. In  $\mathcal{N} = 4$  SYM with adjoint fermions and scalars, the top and the bottom obtain double lines (Fig.1, right) and turn into caps, as a result of which the cylinder turns into a (stretched) sphere (zero handles, zero boundaries).

An analogous result holds for the six point function of external currents in the triple Regge limit. For QCD with fundamental quarks the sphere has three boundaries (for each impact factor, the closed fermion loop defines a boundary), (Fig.3, left) and it has been shown in [10] that the color diagrams fit on the surface of a pair-of-pants (Fig.2). When switching to  $\mathcal{N} = 4$  SYM where fermions and scalars belong to the adjoint representation, the closed lines of the upper and lower impact factors turn into double lines, and the boundaries of the pair-of-pants are replaced by caps, (Fig.3, right). As a result, we again arrive at a sphere, shaped as a pair-of-pants, and we are asked to sum, for the triple Regge limit, diagrams which lie on the surface of this body. As we shall see in the following, there are three distinct classes of diagrams: two of them are the same as in (non-supersymmetric) QCD, whereas the third one is new and has no analog in QCD.

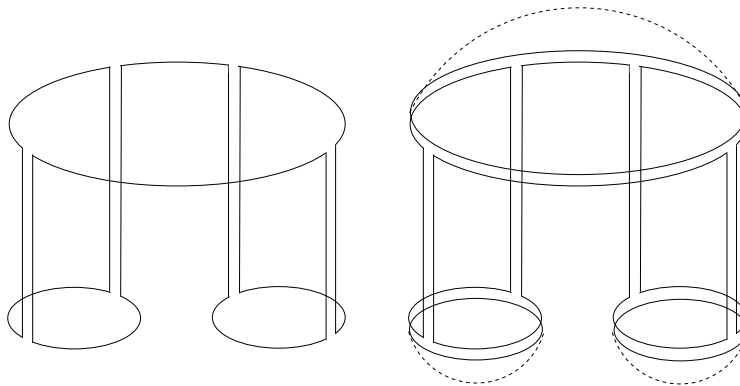


Figure 3: Pair-of-pants topology for the  $3 \rightarrow 3$  amplitude in QCD (left) and in  $\mathcal{N} = 4$  SYM (right)

### 3 Selection of diagrams

Six point amplitudes depend on three energy variables,  $s_1 = (q + p_1)^2$ ,  $s_2 = (q' + p_2')^2$  and  $M^2 = (q + p_1 - p_1')^2$ . The momentum transfer variables are  $t = (q - q')^2$ ,  $t_1 = (p_1 - p_1')^2$  and  $t_2 = (p_2 - p_2')^2$ . The kinematics of a six point amplitude with external  $R$ -currents is illustrated in Fig.4. Then the triple Regge limit is given by

$$s_1 = s_2 \gg M^2 \gg t, t_1, t_2. \quad (8)$$

In the triple Regge limit there is an easy way of computing six point amplitudes of  $R$ -currents, namely we take the triple energy discontinuity in  $s_1$ ,  $s_2$  and  $M^2$ . In lowest order the main ingredients of a

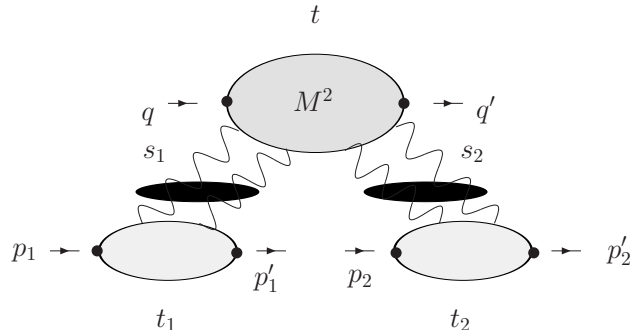


Figure 4: Kinematics of a six point amplitude

diagram are three impact factors and four  $t$ -channel gluons. The impact factors consist of a fermion and a scalar loop and represent the coupling of the  $t$ -channel gluons to the external  $R$ -currents. The insertion of the  $R$ -currents is symbolized by the small black dots in Fig.4. Higher order corrections are taken into account by the production of real gluons in the multi Regge kinematics. In order to form color singlet states which at the top couple to the upper  $R$ -current and at the bottom to two  $R$ -currents, one obtains diagrams with four  $t$ -channel gluons at the lower end and two, three or four  $t$ -channel gluons at the upper end. In particular  $t$ -channel gluons can emerge from produced real gluons and the number of  $t$ -channel gluons can change inside the diffractive system.

We now discuss in the double line notation the relevant diagrams which contribute to the triple Regge limit of the six point correlators of  $R$ -currents. We will closely follow the discussion of [10], and we will use the same notation. In the following double line diagrams we do not show the attached  $R$ -currents, we only consider the gluons and adjoint particle loops.

We begin with a comment on the cylinder in QCD, (Fig.1, left). When replacing, at the top of the cylinder, the fermion in the fundamental representation by an adjoint fermion, we simply draw, above the already existing color line of the fermion, an additional closed color loop which generates an additional factor  $N_c$ . The double line notation now also includes scalar loops. The two  $t$ -channel gluons are attached to the same color line of the closed loop, either to the lower line or to the upper one as shown in Fig.1, right. Diagrams where the two  $t$ -channel lines are attached to different lines lose this additional factor  $N_c$  and are suppressed. As a result of this simple observation, the contribution of the adjoint fermions to the impact factors is proportional to  $N_c$  times that of a fundamental one<sup>1</sup>. In  $\mathcal{N} = 4$  SYM, the four point correlator is of the form  $N_c^2 A_{2 \rightarrow 2}(\lambda)$ , whereas in non-supersymmetric QCD it is of the form  $N_c^0 A_{2 \rightarrow 2}(\lambda)$ .

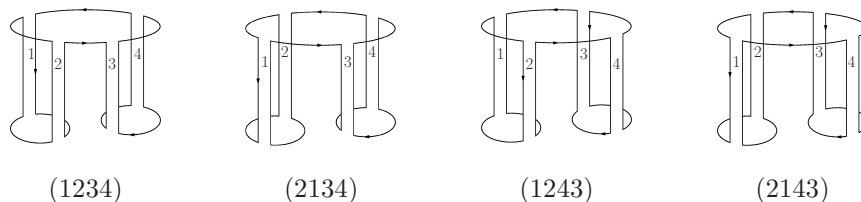


Figure 5: The four different orderings of color factors of the Born-term in QCD with fermions in the fundamental representation of  $SU(N_c)$

<sup>1</sup>This is nothing else but the consequence of the different normalizations of generators. In the fundamental representation we use  $\text{tr}(t^a t^b) = \delta^{ab}$ , whereas in the adjoint representation we have  $\text{tr}(T^a T^b) = N_c \delta^{ab}$ . Note that our normalization of the fundamental generators deviates by a factor 2 from the standard normalization  $\text{tr}(\tau^a \tau^b) = \delta^{ab}/2$ .

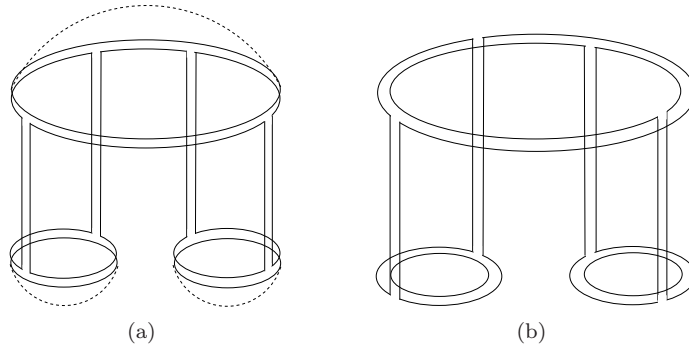


Figure 6: Pair-of-pants topology for the  $3 \rightarrow 3$  amplitude in  $\mathcal{N} = 4$  SYM: (a) a color configuration already present in QCD, and (b) a new one which exists only for adjoint particles

Let us now turn to the six point function. In QCD in lowest order the four  $t$ -channel gluons couple to the upper fermion or scalar loop in all possible ways, all together there are 16 different diagrams. A closer look shows that we have inside the 16 diagrams four different orderings of color matrices. For the lowest order diagrams in the non-supersymmetric QCD case, the four different structures are illustrated in Fig.5.

Switching to  $\mathcal{N} = 4$  SYM, we simply perform, for each of the three impact factors, the substitution we have just described for the BFKL cylinder, and we obtain the additional factor  $N_c^3$ , leading to a result of the order  $N_c^2 \lambda^4$ . Whereas in QCD the analogous lowest order graphs fit on the surface of a pair-of-pants in Fig.2, the diagrams now have the shape of a deformed sphere as shown once again in Fig.6(a). Here both gluon cylinders are coupled to the same line of the upper loop.

A closer inspection shows that, in addition to Fig.6(a), another configuration is possible: without losing a factor  $N_c$ , we can attach one of the cylinders to the outer loop, the other one to the inner loop (Fig.6(b)). This additional piece in the four gluon impact factor which has no counterpart in the fundamental representation, has first been found in [7]. An alternative way of drawing this graph is shown in Fig.7.

In higher order  $\lambda$ , several possibilities arise. We briefly summarize the discussion given in [7]. The general structure of the diagrams is the following: At the upper impact factor we start with a  $t$ -channel state with two, three or four gluons. The propagation of the  $t$ -channel gluons is described by the BKP equations and transition between different states by vertices. We can have  $2 \rightarrow 2$ ,  $2 \rightarrow 3$ , or  $2 \rightarrow 4$  vertices. There is always a lowest interaction between the gluons defined by the  $M^2$ -discontinuity below which the upper cylinder breaks up into two disconnected ones. After this branching vertex the gluons interact only pairwise according to the BFKL equation and are coupled to the two impact factors of the  $R$ -currents at the bottom.

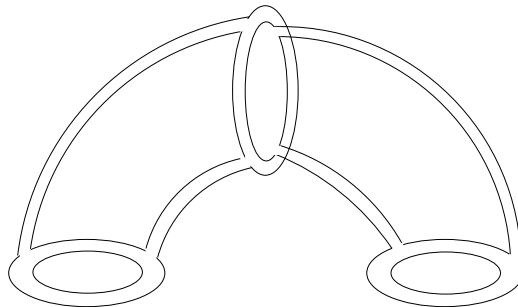


Figure 7: An alternative way of drawing Fig.6(b)

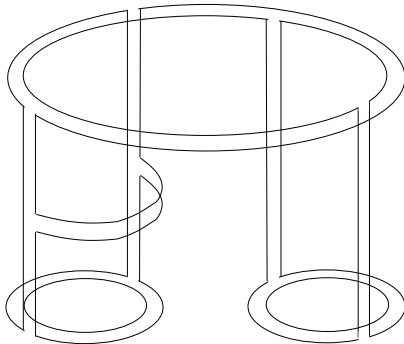


Figure 8: Example of a next-to-leading order diagram of Fig.6(b)

Starting with the one-loop corrections to Fig.6(b), one realizes that it is only possible to insert  $2 \rightarrow 2$  transitions inside the two cylinders: an example is shown in Fig.8. In particular, any rung connecting the two cylinders loses a power of  $N_c$ . As a result, this class of diagrams simply consists of two BFKL Pomeron coupled to the four gluon impact factor, and the resulting amplitude is of the form  $N_c^2 A_{3 \rightarrow 3}(\lambda)$ . This class of diagrams will be named 'direct': the two BFKL Pomerons couple directly to the upper impact factor. As discussed in [10], on the cylinder each gluon rung comes in two different ways, one in front of the cylinder, the other one on the backside. This observation also applies to the  $\mathcal{N} = 4$  SYM case.

Returning to the diagram in Fig.6(a), that is already present in non-supersymmetric QCD, insertion of one additional rung opens two distinct classes of graphs: examples are given in Fig.9, and it is suggestive to name them as 'planar' and 'non-planar', respectively. By definition, planar graphs have the property that, by contracting closed color loops, they can be reduced to the  $\mathcal{N} = 4$  SYM version of the graphs in Fig.5. For the non-planar ones, this is not possible. Beginning with the graph shown in Fig.9b, there is a new class of diagrams which cannot be deformed into planar graphs.

Altogether we have to distinguish three different types of diagrams: the direct, the planar, and the non-planar diagrams. In the first case, the direct diagrams, the lowest interaction between the two cylinders, which defines the value of the diffractive mass  $M^2$ , is the upper impact factor itself. The four gluons couple directly the upper loop without interaction between the two disconnected BFKL Pomerons.

The second type of diagrams are planar diagrams: At the upper loop they start with two, three, or four  $t$ -channel gluons. These gluons undergo transitions by  $2 \rightarrow 2$ ,  $2 \rightarrow 3$ , or  $2 \rightarrow 4$  vertices,

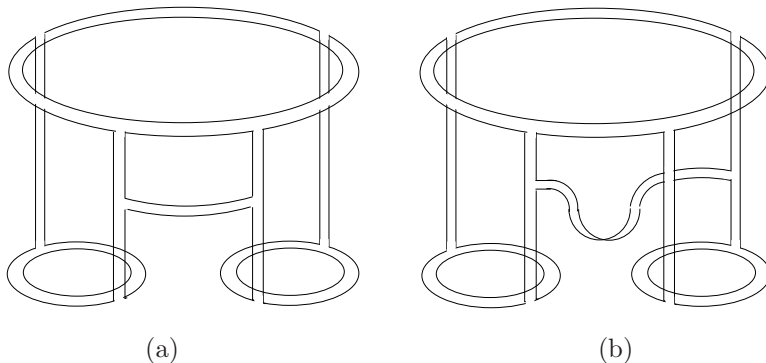


Figure 9: Two classes of diagrams: planar graphs (a) and non-planar graphs (b)

respectively. One of these transitions is the branching vertex below which we always have four gluons but each two gluons only interact pairwise after the branching vertex. They form once again the two non-interacting BFKL Pomerons.

The last possibility are non-planar diagrams. At the upper loop they can also start with two, three, or four  $t$ -channel gluons and the structure above the branching vertex is the same as for planar diagrams. But the branching vertex itself now provides a non-planar structure. Below this non-planar vertex the known disconnected BFKL cylinders show up.

## 4 Analytic expressions

Let us now turn to analytic expressions. It is convenient to use the analytic representations of multi-particle amplitudes. A detailed discussion can be found in [13]. We restrict ourselves to those contributions which have a non-vanishing discontinuity in  $M^2$ . In the triple Regge limit, Eq.(8), we have for the  $3 \rightarrow 3$  amplitude:

$$T_{3 \rightarrow 3}(s_1, s_2, M^2 | t_1, t_2, t) = \frac{s_1 s_2}{M^2} \int \frac{d\omega_1 d\omega_2 d\omega}{(2\pi i)^3} s_1^{\omega_1} s_2^{\omega_2} (M^2)^{\omega - \omega_1 - \omega_2} \xi(\omega_1) \xi(\omega_2) \xi(\omega, \omega_1, \omega_2) \cdot F(\omega, \omega_1, \omega_2 | t, t_1, t_2) + \dots \quad (9)$$

The dots represent three further terms that appear in the triple Regge limit: they do not contribute to the  $M^2$ -discontinuity. The signature factors are given by

$$\xi(\omega) = -\pi \frac{e^{-i\pi\omega} - 1}{\sin(\pi\omega)} \quad \text{and} \quad \xi(\omega, \omega_1, \omega_2) = -\pi \frac{e^{-i\pi(\omega - \omega_1 - \omega_2)} - 1}{\sin \pi(\omega - \omega_1 - \omega_2)}. \quad (10)$$

As discussed in the previous section, for the computation we have taken the triple energy discontinuity of the amplitude in  $s_1$ ,  $s_2$ , and  $M^2$ :

$$\text{disc}_{s_1} \text{disc}_{s_2} \text{disc}_{M^2} T_{3 \rightarrow 3} = \pi^3 \frac{s_1 s_2}{M^2} \int \frac{d\omega_1 d\omega_2 d\omega}{(2\pi i)^3} s_1^{\omega_1} s_2^{\omega_2} (M^2)^{\omega - \omega_1 - \omega_2} \cdot F(\omega, \omega_1, \omega_2 | t_1, t_2, t), \quad (11)$$

which, via a triple Mellin transform, is related to the partial wave  $F(\omega, \omega_1, \omega_2 | t_1, t_2, t)$ . For the calculation of the triple discontinuity we have used unitarity integrals, and the summation of the diagrams has been performed by means of integral equations. These integral equations can be solved and the solution is, due to the resulting bootstrap, far more simpler than suggested by the structure of the underlying diagrams. Details can be found in [10], and we only describe the results.

Our result for the sum of the diagrams which fit on the surface of the deformed sphere (Fig.6) is given by the sum of three terms which sum different classes of diagrams: planar diagrams, non-planar diagrams, and direct diagrams:

$$T_{3 \rightarrow 3} = T_{3 \rightarrow 3}^{(P)} + T_{3 \rightarrow 3}^{(\text{NP})} + T_{3 \rightarrow 3}^{(\text{DIR})}. \quad (12)$$

The three different parts are illustrated in Fig.10. In the triple Regge limit, Eq.(8), the partial waves factorize and consist of several building blocks. In our case we encounter two-gluon impact factors, BFKL Green's functions, and a triple vertex which connects them. The two-gluon impact factors,  $\mathcal{D}_{(2;0)}$ , describe the coupling to the external  $R$ -currents. For  $\mathcal{N} = 4$  SYM they have been computed in [2]. They contain both fermions and scalar in the adjoint representation<sup>2</sup>.

Let us go into some detail. For the sum of the first two terms we use the representation Eq.(9) and write

$$F(\omega, \omega_1, \omega_2) = F^{(P)}(\omega, \omega_1, \omega_2) + F^{(\text{NP})}(\omega, \omega_1, \omega_2). \quad (13)$$

<sup>2</sup>For the large  $N_c$  analysis it is convenient to absorb an additional factor  $N_c$  into the impact factor. With the two-gluon  $R$ -current impact factor of [2] given by  $\Phi^{aa'} = \delta^{aa'} \Phi$ , we use in the following  $\mathcal{D}_{(2;0)} = N_c \Phi$ , which is then proportional to  $\lambda N_c$ .



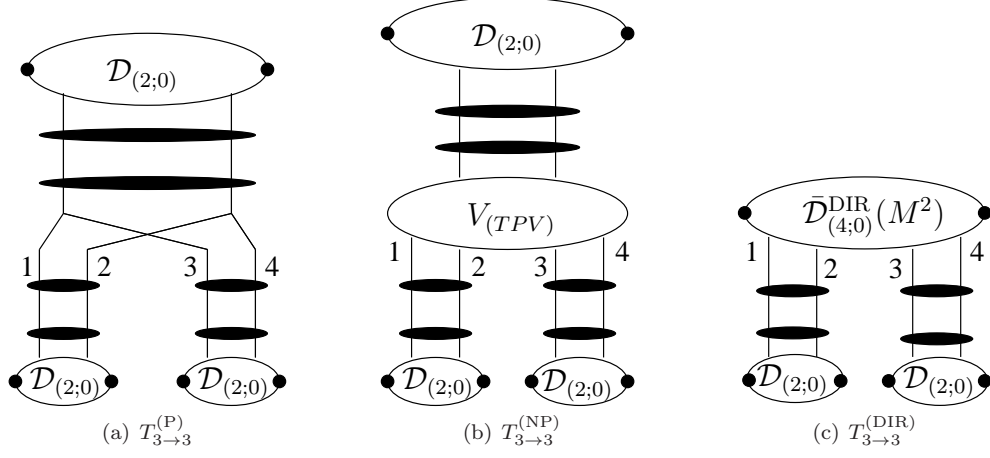


Figure 10: The three different parts of the six point function  $T_{3 \rightarrow 3}$

As seen in Fig.10, the impact factors appear at the three different ends of the diagrams, and they are connected by BFKL Green's functions and a triple vertex in the center. The two terms differ from each other by the form of the triple vertex: in the second term, the vertex is due to the non-planar diagrams and coincides with the triple Pomeron vertex found in QCD. The first term which results from the planar diagrams is a direct consequence of the reggeization of the gauge boson. The partial wave has the form:

$$F^{(P)}(\omega, \omega_1, \omega_2) = 4\mathcal{D}_2^{(12)}(\omega_1) \otimes_{12} \mathcal{D}_2^{(34)}(\omega_2) \otimes_{34} \left( \bar{D}_{(4;0)}(\omega) + [\omega - \omega_1 - \omega_2] \frac{\bar{\lambda}}{N_c} V^R \otimes \mathcal{D}_2(\omega) \right) \quad (14)$$

with  $\bar{\lambda} = \lambda/2$ . The convolution symbol is defined as

$$\otimes_{12} = \int \frac{d^2 \mathbf{k}_1}{(2\pi)^3 \mathbf{k}_1^2 \mathbf{k}_2^2}, \quad (15)$$

where  $\mathbf{k}_1$  and  $\mathbf{k}_2$  are the transverse momenta of the gluons 1 and 2. In Eq.(14) we have introduced the three functions  $\mathcal{D}_2(\omega)$ ,  $\mathcal{D}_2(\omega_1)$ ,  $\mathcal{D}_2(\omega_2)$  which combine the three impact factors  $D_{(2;0)}$  with their adjacent BFKL Green's functions. The subscript 12 at the convolution symbol indicates that the two gluon amplitude  $\mathcal{D}_2^{(12)}(\omega_1)$  has to be contracted with the  $t$ -channel gluons 1 and 2. Similarly,  $\otimes_{34}$  belongs to the gluons 3 and 4. An analytic expression for the triple vertex  $V^R$  can be found in [10].

The second part of the partial wave takes the form

$$F^{(NP)}(\omega, \omega_1, \omega_2) = 4\mathcal{D}_2^{(12)}(\omega_1) \otimes_{12} \mathcal{D}_2^{(34)}(\omega_2) \otimes_{34} \frac{\bar{\lambda}^2}{N_c} V_{(TPV)} \otimes \mathcal{D}_2(\omega). \quad (16)$$

The main ingredient here is the triple Pomeron vertex  $V_{(TPV)}$ , which as described in [10], Eq.(87), coincides with the large- $N_c$  limit of the QCD result of [6]. Interesting enough, the first term,  $F^{(P)}$ , is present only in the triple Regge limit with fixed  $M^2$ . As explained in [7, 14], after integration over  $M^2$  and  $t_1$  and  $t_2$ , our six point function can be viewed as a part of the scattering of the upper  $R$ -current on a loosely bound state of the two lower  $R$ -currents: in this case this part of the triple vertex disappears and turns into a special contribution to the initial conditions of the evolution of a BFKL Green's function, and only the triple Pomeron vertex remains (a detailed discussion of this mechanism is given in [6], after Eq.(4.14)).

Finally, we have the third part in Fig.10,  $T_{3 \rightarrow 3}^{(DIR)}$ , where the two BFKL Green's functions couple directly to the upper 'unintegrated' impact factor,  $\bar{D}_{(4;0)}^{DIR}(M^2)$ . Here the dependence upon  $M^2$  is

contained inside  $\bar{\mathcal{D}}_{(4;0)}^{\text{DIR}}$ , and instead of Eq.(9) we use

$$T_{3 \rightarrow 3}^{(\text{DIR})}(s_1, s_2, M^2 | t_1, t_2, t) = s_1 s_2 \int \frac{d\omega_1 d\omega_2}{(2\pi i)^2} \left(\frac{s_1}{M^2}\right)^{\omega_1} \left(\frac{s_2}{M^2}\right)^{\omega_2} \xi(\omega_1) \xi(\omega_2) F^{(\text{DIR})}(M^2, \omega_1, \omega_2 | t, t_1, t_2). \quad (17)$$

The partial wave is given by

$$F^{(\text{DIR})}(M^2, \omega_1, \omega_2 | t, t_1, t_2) = 4 \mathcal{D}_2^{(12)}(\omega_1) \otimes_{12} \mathcal{D}_2^{(34)}(\omega_2) \otimes_{34} \bar{\mathcal{D}}_{(4;0)}^{\text{DIR}}(M^2). \quad (18)$$

The direct coupling of the amplitudes  $\mathcal{D}_2^{(12)}(\omega_1)$  and  $\mathcal{D}_2^{(34)}(\omega_2)$  to the upper loop is described by the 'unintegrated' impact factor  $\bar{\mathcal{D}}_{(4;0)}^{\text{DIR}}(M^2)$  which has both right hand and left hand cuts in  $M^2$ . In contrast to the 'normal' impact factors which are integrated over the mass  $M^2$ , in this case the coupling to the upper  $R$ -current is with fixed  $M^2$ . Restricting ourselves to the forward case with zero momentum transfers  $t = t_1 = t_2 = 0$ , i.e.  $\mathbf{k}_1 = -\mathbf{k}_2 = \mathbf{k}$  and  $\mathbf{k}_3 = -\mathbf{k}_4 = \mathbf{k}'$ , we obtain after integration over the angle  $\varphi$  and  $\varphi'$  of the vector  $\mathbf{k}$  and  $\mathbf{k}'$  respectively,

$$\begin{aligned} F^{(\text{DIR})}(M^2, \omega_1, \omega_2 | 0, 0, 0) &= \\ &= 4 \int \frac{d\mathbf{k}^2}{(2\pi)^3 \mathbf{k}^4} \int \frac{d\mathbf{k}'^2}{(2\pi)^3 \mathbf{k}'^4} \mathcal{D}_2^{(12)}(\omega_1, \mathbf{k}^2) \mathcal{D}_2^{(34)}(\omega_2, \mathbf{k}'^2) \bar{\mathcal{D}}_{(4;0)}^{\text{DIR}}(\mathbf{k}^2, \mathbf{k}'^2, M^2), \end{aligned} \quad (19)$$

where (see also [7]):

$$\bar{\mathcal{D}}_{(4;0)}^{\text{DIR};hh'}(\mathbf{k}^2, \mathbf{k}'^2, M^2) = \frac{g^4}{32} \frac{1}{M^2} \delta_{hh'} \int_0^1 d\alpha I_v(\alpha, \mathbf{k}^2, M^2) I_v(\alpha, \mathbf{k}'^2, M^2) \quad (20)$$

and

$$\bar{\mathcal{D}}_{(4;0)}^{\text{DIR};LL}(\mathbf{k}^2, \mathbf{k}'^2, M^2) = \frac{g^4}{32} Q^2 \int_0^1 d\alpha \alpha^2 (1-\alpha)^2 I_s(\alpha, \mathbf{k}^2, M^2) I_s(\alpha, \mathbf{k}'^2, M^2). \quad (21)$$

Here the dependence on  $M^2$  is explicit.  $L$  and  $h$  denote the different polarizations of the incoming and outgoing  $R$ -currents. The functions  $I_v$  and  $I_s$  are given by

$$I_v(\alpha, \mathbf{k}^2, M^2) = \left( \frac{Q^2 - M^2}{Q^2 + M^2} - \frac{\mathbf{k}^2 + \alpha(1-\alpha)(Q^2 - M^2)}{\sqrt{(\mathbf{k}^2 + \alpha(1-\alpha)(Q^2 - M^2))^2 + 4\alpha^2(1-\alpha)^2 M^2 Q^2}} \right), \quad (22)$$

and

$$I_s(\alpha, \mathbf{k}^2, M^2) = 2 \left( \frac{1}{\sqrt{(\mathbf{k}^2 + \alpha(1-\alpha)(Q^2 - M^2))^2 + 4\alpha^2(1-\alpha)^2 M^2 Q^2}} - \frac{1}{\alpha(1-\alpha)(Q^2 + M^2)} \right). \quad (23)$$

A final comment on  $F^{(\text{DIR})}$ : Compared to  $F^{(\text{P})}$  and  $F^{(\text{NP})}$  this term is sub-leading for large values of  $M^2$ . It therefore contributes in the region of low-diffractive mass  $M^2$ , whereas the region of high-diffractive mass  $M^2$  is governed by  $F^{(\text{P})}$  and  $F^{(\text{NP})}$ .

The expressions listed in this section can directly be compared with results obtained from the analysis of Witten diagrams in the strong coupling regime [15].

## 5 Conclusions

In this letter we have presented results for the six point  $R$ -current correlator in  $\mathcal{N} = 4$  SYM in the triple Regge limit. In view of the AdS/CFT correspondence, which relates the large- $N_c$  limit of  $\mathcal{N} = 4$

SYM to a string theory in  $AdS_5$ , we have concentrated on those diagrams which fit on the surface of a sphere. This generalizes an earlier calculation in non-supersymmetric QCD, where the leading diagrams fit on the surface of a pair-of-pants.

Our result consists of three terms which correspond to different classes of color diagrams. Each term is composed of several building blocks: impact factors, triple vertex, and BFKL Green's functions. They should be compared with corresponding Witten diagrams in the strong coupling region. Further work along these lines is in progress [15].

## References

- [1] J. M. Maldacena, *Adv. Theor. Math. Phys.* **2** (1998) 231 [*Int. J. Theor. Phys.* **38** (1999) 1113] [arXiv:hep-th/9711200]; E. Witten, *Adv. Theor. Math. Phys.* **2** (1998) 253 [arXiv:hep-th/9802150]; S. S. Gubser, I. R. Klebanov and A. M. Polyakov, *Phys. Lett. B* **428** (1998) 105 [arXiv:hep-th/9802109].
- [2] J. Bartels, A.-M. Mischler and M. Salvadore, *Phys. Rev. D* **78**, 016004 (2008) [arXiv:0803.1423 [hep-ph]].
- [3] L. N. Lipatov, *Sov. J. Nucl. Phys.* **23** (1976) 338 [*Yad. Fiz.* **23** (1976) 642]; V. S. Fadin, E. A. Kuraev and L. N. Lipatov, *Phys. Lett. B* **60** (1975) 50; *Sov. Phys. JETP* **44** (1976) 443 [*Zh. Eksp. Teor. Fiz.* **71** (1976) 840]; *Sov. Phys. JETP* **45** (1977) 199 [*Zh. Eksp. Teor. Fiz.* **72** (1977) 377]; I. I. Balitsky and L. N. Lipatov, *Sov. J. Nucl. Phys.* **28** (1978) 822 [*Yad. Fiz.* **28** (1978) 1597].
- [4] J. Bartels, J. Kotanski, A.-M. Mischler, V. Schomerus, in preparation.
- [5] L. N. Lipatov, *Phys. Lett. B* **116**, 411 (1982), A. V. Kotikov, L. N. Lipatov, A. I. Onishchenko and V. N. Velizhanin, *Phys. Lett. B* **595** (2004) 521 [Erratum-ibid. B **632** (2006) 754] [arXiv:hep-th/0404092], R. C. Brower, J. Polchinski, M. J. Strassler and C. I. Tan, *JHEP* **0712** (2007) 005 [arXiv:hep-th/0603115].
- [6] J. Bartels and M. Wusthoff, *Z. Phys. C* **66** (1995) 157.
- [7] J. Bartels, C. Ewerz, M. Hentschinski, A.-M. Mischler, to be published.
- [8] L. N. Lipatov, *JETP Lett.* **59** (1994) 596 [*Pisma Zh. Eksp. Teor. Fiz.* **59** (1994) 571]; L. D. Faddeev and G. P. Korchemsky, *Phys. Lett. B* **342** (1995) 311 [arXiv:hep-th/9404173].
- [9] J. Bartels, *Nucl. Phys. B* **175** (1980) 365; J. Kwiecinski and M. Praszalowicz, *Phys. Lett. B* **94** (1980) 413.
- [10] J. Bartels and M. Hentschinski, arXiv:0903.5464 [hep-ph].
- [11] G. 't Hooft, *Nucl. Phys. B* **72** (1974) 461.
- [12] G. 't Hooft, *Nucl. Phys. B* **75** (1974) 461.
- [13] R. C. Brower, C. E. DeTar and J. H. Weis, *Phys. Rept.* **14** (1974) 257.
- [14] J. Bartels, M. Salvadore and G. P. Vacca, *JHEP* **0806**, 032 (2008) [arXiv:0802.2702 [hep-ph]].
- [15] J. Bartels, J. Kotanski, A.-M. Mischler, V. Schomerus, in preparation.